

Influence of Conical Wire Array Geometry on Flow and Temperature Profiles Measured via Thomson Scattering and Optical Techniques

Luisa Izquierdo^{1,*}, Felipe Veloso^{1,†}, Miguel Escalona¹, Vicente

Valenzuela-Villaseca², Gonzalo Avaria³, Julio Valenzuela¹

¹*Instituto de Física, Pontificia Universidad Católica de Chile, Santiago 7820436, Chile.*

²*Department of Astrophysical Sciences, Princeton University, Princeton, New Jersey 08544, USA.*

³*Departamento de Física, Universidad Técnica Federico Santa María, Santiago 8940897, Chile**

Conical wire arrays with different opening angles are used as load of a 400kA, 1kA/ns generator. The differences in opening angle allow the study of the influence of the array geometry on the jet properties. The characterization of the jets is performed using a combination of advanced diagnostic techniques, including moiré schlieren deflectometry, visible self-emission spectroscopy, and optical Thomson scattering. The results reveal that, under the experimental conditions, the plasma jets exhibit electron temperatures ranging from 8 to 17 eV, increasing along the axial direction. In contrast, the ion temperature decreases from approximately 35 eV near the base of the jet to about 20 eV at higher axial positions. The electron density profile peaks at $\sim 4 \times 10^{18} \text{ cm}^{-3}$ in the central lower region of the jet and decreases with height exponentially with a characteristic length $L_n = 2.86 \text{ mm}$. This behavior is reproducible and independent of the conical array geometry. However, the cone opening angle significantly affects the jet propagation velocity, with larger opening angles producing higher axial velocities ($V_{\phi=40^\circ} \approx 125 \pm 3 \text{ km/s}$, $V_{\phi=20^\circ} \approx 98 \pm 5 \text{ km/s}$), demonstrating that the cone geometry provides effective control over the jet propagation velocity.

I. INTRODUCTION

Astrophysical plasma jets [1] are ubiquitous phenomena observed across a wide range of environments, including active galactic nuclei (AGNs) [2], young stellar objects (YSOs) [3], and planetary nebulae (PNs) [4]. These jets typically manifest as highly collimated, supersonic plasma outflows, playing critical roles in the transport of mass, energy, and magnetic fields over large astrophysical scales.

Motivated by the astrophysical relevance of plasma jets, a variety of laboratory platforms have been developed to generate and study scaled analogs of these phenomena. Experiments based on conical wire arrays [5–7], radial wire arrays [8, 9], and gas-puff Z-pinchs [10] have all successfully produced radiatively cooled, magnetically collimated plasma jets that satisfy scaling laws relevant to astrophysical systems. These laboratory experiments have enabled the study of jet propagation, stability, episodic ejection, interaction with ambient media, and radiative cooling under controlled conditions.

Despite differences in experimental implementation, many of these platforms share common features: the generation of a dense plasma column, the presence of a surrounding magnetic field that assists in jet collimation, and the occurrence of radiative cooling that influences jet morphology. These similarities have allowed experimental studies to explore universal aspects of plasma jet physics across a range of conditions.

Among these platforms, plasma jets produced by conical wire array Z-pinchs stand out for their high degree of collimation and relevance to young stellar object out-

flows [7, 11]. However, despite significant advances, experimental characterizations of these laboratory plasma jets have largely relied on indirect diagnostic methods. Most notably, time-resolved laser probing (e.g., interferometry and schlieren) has been used to infer axial density variations, while self-emission imaging has provided qualitative information about jet morphology and dynamics [11, 12]. These techniques, although powerful, do not directly measure key plasma parameters such as the flow velocity or internal gradients, often leading to ambiguities in the interpretation of jet structure. For instance, axial variations observed in interferometry can result from either real flow dynamics or geometric zipper effects, and numerical simulations predict axial velocity gradients [13] that remain unobserved experimentally.

In addition to diagnostic limitations, the standard conical wire array configuration allows significant lateral plasma inflows toward the axis during jet formation. These inflows, which can contribute to the closure of electrical current through the plasma column [14, 15], complicate the interpretation of experimental results and may artificially enhance jet stability and density profiles.

In this work, to address these questions, we performed a detailed experimental study of plasma jets emitted by aluminum conical wire arrays driven by the Llampudken pulsed power generator. This study combines Thomson scattering, optical self-emission spectroscopy, and moiré schlieren deflectometry to spatially resolve plasma density, temperature, and flow velocity. Moreover, to improve jet purity and reproducibility, an aperture was incorporated into the upper electrode to filter out parasitic plasma flows originating from the wire ablation phase before the formation of the main jet. Finally, by varying the opening angle of the conical array, we investigate how geometrical factors influence the plasma parameters of the emitted jets, providing new insights into the for-

* luisa.izquierdo@uc.cl, fveloso@uc.cl

mation mechanisms and flow dynamics relevant to laboratory astrophysics experiments.

II. EXPERIMENTAL SETUP AND DIAGNOSTICS

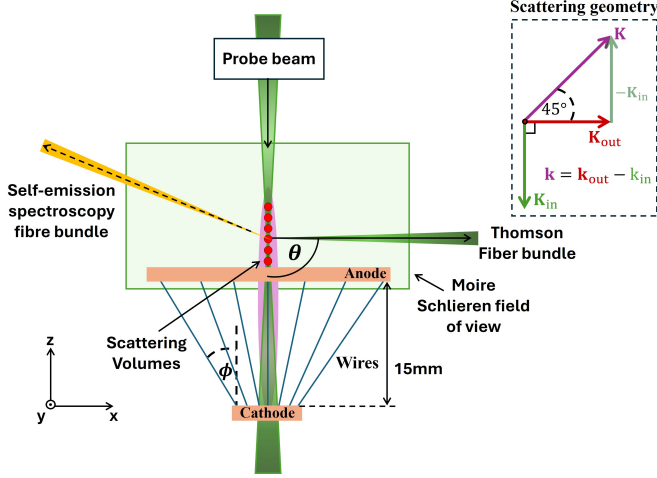


FIG. 1. Schematic diagram of experimental setup. Conical wire array opening angle is determined by the angle ϕ . TS volumes are overlaid in red circles (not scale). Continuous arrows indicate the scattering geometry. Dashed arrows show the collection direction of the spectroscopy. Additionally, the field of view of side-on moiré schlieren.

Plasma jets are generated when the plasma ablated from the wires is accumulated at the axis of the configuration, and later expelled axially due the zippering effect of the conical wire array when used as the load of the ~ 400 kA, ~ 1 kA/ns current pulse of the Llampudken pulsed-power generator [16]. The conical wire array consists of sixteen equally spaced aluminium wires of $50 \mu\text{m}$ diameter each. The total height of the array is given by interelectrode separation, which is set constant at 15 mm in all the experiments reported here. A schematic of the experimental setup is shown in Fig. 1.

To experimentally investigate the effect of the opening angle of the conical wire array (ϕ , measured with respect to the vertical, as shown in Fig. 1), three different angles are studied: $\phi = 20^\circ$, 30° , and 40° . In all these cases, the cathode diameter remains fixed at 7 mm while the anode diameter is adjusted accordingly to achieve the desired opening angles. Hence, anode diameters of 17.9 mm, 24.3 mm, and 32.1 mm, are used corresponding to the respective opening angles. In addition, the array load is covered by a 3 mm thick metallic lid having a central aperture of 5 mm in diameter. This aperture is geometrically designed for limiting the plasma emerging above the interelectrode region (above anode). Using this aperture, the ablated plasma emerging from the wires driven by the Lorentz force (i.e., plasma flares propagating perpendicular to the wires) cannot pass directly through the

lid aperture. This is true for the $\phi = 20^\circ$ and $\phi = 30^\circ$ cases. For the $\phi = 40^\circ$, the ablated plasma can reach at most 2.09 mm over the anode lid. On the contrary, the plasma jet can pass through the central aperture due to its axial propagation. Therefore, the measurements performed above anode (lid) surface correspond exclusively to the plasma jet and not to the ablation flares emitted from the wires. Throughout this article, temporal reference $t = 0$ is considered when current begins to flow through the load. Moreover, axial propagation of the jet is measured by considering $z = 0$ as the anode surface above the interelectrode region.

In the experiments, the overall structure and plasma parameters are investigated using a comprehensive multi-diagnostic suite. Moiré schlieren deflectometry [17] is used to measure the line integrated electron density gradient in the side on direction. It is carried out using the second (532 nm) harmonic of a Nd:YAG laser. The moiré fringe pattern is formed with two Ronchi gratings with a ruling of 20 lines/mm, separated by 1.57 cm, corresponding to three Talbot distances and rotated by an angle $\psi = 10^\circ$ with respect to each other [18]. Structures in the moiré schlieren images are eliminated using spatial Fourier filters that selects the frequencies corresponding to the moiré pattern. The shift of moiré fringes is proportional to the line integrated electron density gradient $\int \nabla n_e dl$ and the volumetric electron density n_e can be reconstructed using an onion-peeling inversion method [19], considering axial symmetry. In this setup, electron densities above $6.7 \times 10^{17} \text{ cm}^{-3}$ can be measured. As shown in Fig.1, the laser beam is aligned side-on to the experiment, passing over the top edge of the upper electrode to obtain a cross-sectional view of the plasma jet.

In addition, visible self-emission spectroscopy and optical Thomson Scattering (TS) are employed, both providing spatial resolution along the axial propagation direction of the plasma jet. TS is used to measure the flow velocity and electron and ion temperatures. A laser beam (532 nm, 1 J, 4 ns) is focused along the plasma jet propagation axis and scattered light was collected by a fiber optic bundle with an scattering angle $\theta = 90^\circ$, as shown in Fig. 1. The fiber bundle consist of a linear array of 25 fiber optics ($200 \mu\text{m}$ diameter, $200 \mu\text{m}$ fiber to fiber distance), and light is collected at 25 distinct axial positions. The Thomson scattering collection volume is determined by the cross-sectional area of the laser beam and the optical collection volume length, given by $l = 2.1 \times 200 \mu\text{m} = 420 \mu\text{m}$. The collected light is transmitted to a 500 mm focal length spectrometer (SpectraPro HRS-500) equipped with a $50 \mu\text{m}$ entrance slit and a 2400 l/mm grating. Spectra are recorded using a gated ICCD camera (Stanford 4 Picos) with an exposure time of 6 ns.

Similarly, self-emission spectra are acquired using a linear fiber bundle positioned to observe the same regions diagnosed with TS. The fiber bundle consists of $25 \times 200 \mu\text{m}$ diameter fibers, aligned vertically above the anode of the conical wire array along the jet propagation path,

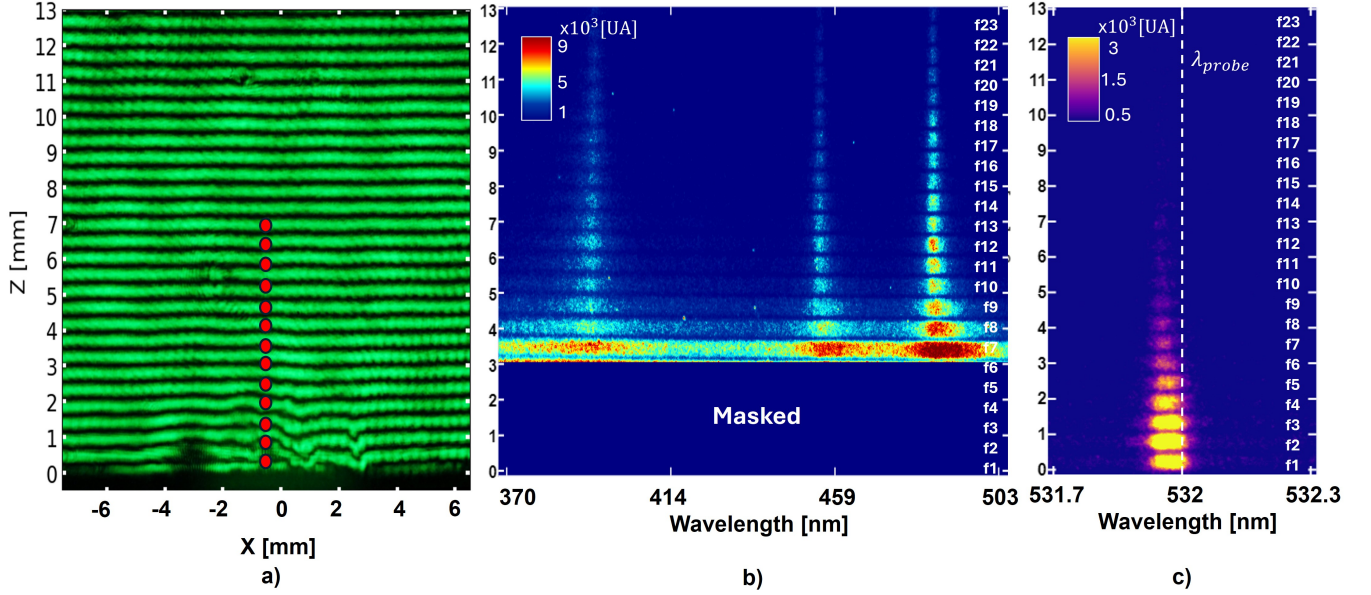


FIG. 2. Raw experimental data of a plasma jet emitted by a 20° conical wire array at 450ns. TS volumes are overlaid in red circles into the side on moiré pattern a). The information was measured just above the anode of the conical wire array ($Z = 0$). b) Visible self-emission spectrum. c) Thomson scattering spectrum of the fiber bundle A. white dashed line indicate the probe wavelength.

with an approximate magnification of 2.1. The collected emission is analyzed using a 500 mm focal length spectrometer equipped with a 150 l/mm grating. Spectra were recorded using a gated ICCD camera (Andor iStar) with an exposure time of 3 ns, covering the wavelength range 365 – 510 nm, where Al-III spectral lines are present.

III. RESULTS

Fig. 2 shows raw data of a plasma jet emitted by a 20° conical wire array, at $t \sim 450$ ns after current discharge. By combining the results of different diagnostics, a plasma jet characterization up to 14 mm above anode surface is achieved.

Raw deflectometry data (Fig.2a) is analyzed using the TNT code [20] to obtain a 1D phase shift of the moiré pattern. In order to assess cylindrical symmetry, we analyze moiré schlieren at both sides of the symmetry axis individually. As shown in Figure 3, the average electron density profile differ less than 5% from each side, demonstrating that cylindrical symmetry assumption is valid. Our moiré measurements reveal a radial electron density profile that peaks in the propagation axis in $n_e^{\phi=20^\circ}(t = 450 \text{ ns}) = (4.0 \pm 0.2) \times 10^{18} \text{ cm}^{-3}$ and radially decrease.

Nevertheless, density measurements using moiré deflectometry are limited by the ability to detect fringe shifts in the pattern. To extend the axial range of density determination, we complement moiré data with spec-

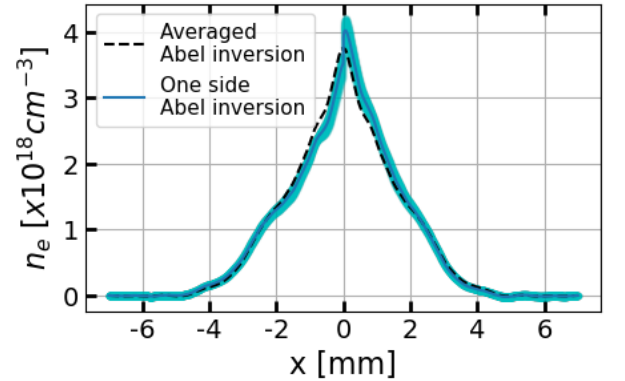


FIG. 3. Abel inverted electron density obtained with moiré schlieren deflectometry measurement at ~ 450 ns plasma jet of a 20° conical array.

troscopy. Figure 2b presents raw self-emission spectral data of the plasma jet, where three emission lines corresponding to Al-III transitions can be clearly distinguished. It is observed that the width of the emission lines varies with the axial position. The lines are broader at lower axial positions (closer to the anode) and gradually narrow at higher positions along the z -axis. This behavior indicates a decreasing trend in electron density as a function of height.

The full width at half maximum (FWHM) of the Al-III emission line at 452.9 nm is measured using a Lorentzian fit to the spectral data (red dashed lines in Fig. 4). Af-

ter correction for instrumental broadening, local electron density values are obtained as a function of axial position by evaluating the Stark broadening relation in the regime where broadening is dominated by electron collisions [21, 22]. A Stark parameter of $\omega = 0.134 \pm 0.025$ pm was used [23].

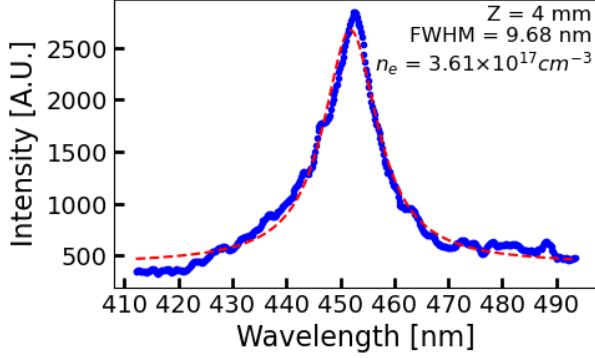


FIG. 4. Characteristic spectral emission line at 452.8 nm (blue dots). Red dashed lines show the lorentzian fit used to determine the FWHM used to estimate stark broadening.

By combining the deflectometry and spectroscopy method, the peak electron density as a function of the axial position (i.e., $n_e^{max}(z)$) is obtained and shown in Fig. 5. Electron density values obtained from both methods exhibit good agreement in the overlapping measurement regions, which indicate consistency in the applied methods.

From Fig 5, it can be seen that peak electron density reaches maximum at the base of the jet near the anode (i.e., closer to the conical array load) reaching a maximum of approximately $4 \times 10^{18} \text{ cm}^{-3}$. At higher axial positions, the electron density decreases, reaching approximately $6 \times 10^{16} \text{ cm}^{-3}$ at $z \approx 13 \text{ mm}$. Moreover, peak density decays exponentially with axial position as $n_e^{max}(z) \propto e^{-z/L_n}$ with $L_n = 2.86 \text{ mm}$. Therefore we consider L_n as a characteristic axial density gradient scale length. Furthermore, electron density remains within the same magnitude regardless of the opening angle ϕ .

On the other hand, TS spectra are analyzed using a bayesian inference method, as described in [24]. Using these data, velocity and temperature measurements were obtained from 10 scattering volumes (red circles in the Fig. 2a).

The flow velocity of the plasma jet was determined from the Doppler shift of the scattered spectra. As shown in Fig.6, the flow velocity increases approximately linearly with the axial position, a behavior observed consistently across all opening angles studied. The rate of increase in flow velocity with axial position is higher for larger ϕ , with an increment of approximately $3 \text{ km s}^{-1}/\text{mm}$ for every 10° increase in ϕ . This results in a maximum velocity of $125 \pm 3 \text{ km/s}$ at $z = 6 \text{ mm}$ for $\phi = 40^\circ$, compared to $98 \pm 5 \text{ km/s}$ at the same position

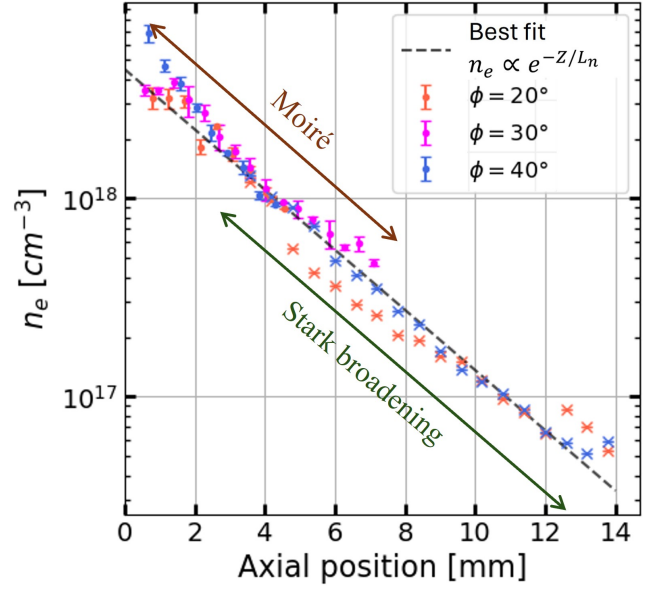


FIG. 5. Peak electron density profile as a function of axial position (z) at the jet axis. for three different conical wire array opening angles. Dot markers represent measurements obtained using moiré Schlieren deflectometry, while x-markers indicate results from Stark broadening. The dashed black line shows the best fit to the 20° - cone data, given by $n_e = 4.5e^{-0.35z}$.

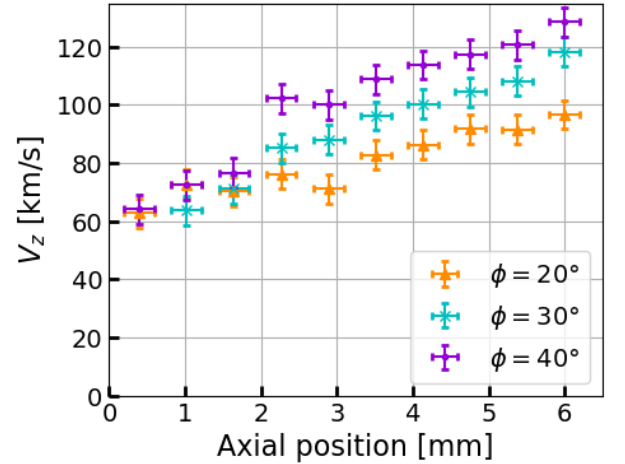


FIG. 6. Axial velocity profile of the plasma jet for different opening angles, 450ns after the beginning of current discharge

for $\phi = 20^\circ$. These results indicate that the inclination angle of the conical wire array serves as a control parameter for the propagation velocity of the jet.

The intensity of the scattered spectra decreases at higher axial positions, consistent with the electron density profile obtained. Throughout the observed range, the spectra do not exhibit ion-acoustic features, likely because $ZT_e < 3T_i$ [25], resulting in a scattered spectrum that remains nearly Gaussian.

Due to the absence of ion-acoustic features, an exact measurement of the electron temperature (T_e) is not possible. Instead, the TS fitting was constrained using the electron density obtained from a combination of deflectometry and spectral data. Under these constraints, TS provides the ion temperature (T_i), and subsequently, an upper limit for T_e . Then we vary T_e in the fit until the onset of a double-peaked spectral feature is observed. Based on the fitted values, a lower bound for the average ionization state (Z) is established

Fig. 7 shows an example of the spectrum obtained and its corresponding fit for a 40° cone, collected by a single fiber at approximately 2 mm from the anode and ~ 450 ns after the current discharge.

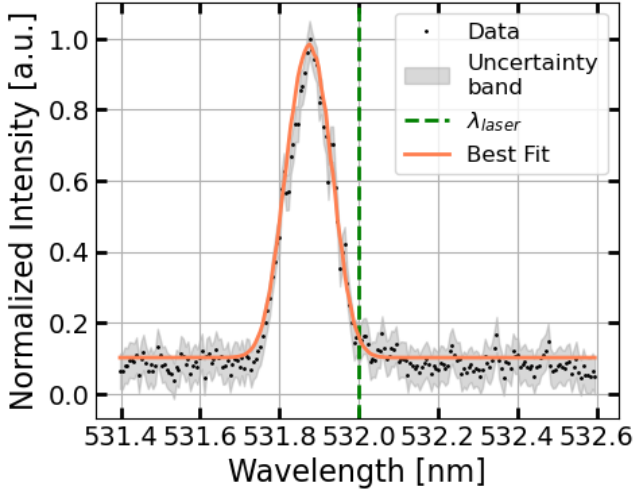


FIG. 7. TS spectrum of the 40° cone, collected by a single fiber at $Z \approx 2$ mm from the anode, ~ 450 ns after the current discharge. The data are shown in black dots and the best fit in the continuum orange line

The plasma parameters obtained for the jet emitted by a 40° conical wire array are summarized in Fig. 8. It is observed that, for most axial positions, $T_i > T_e$. This temperature difference gradually decreases along the axial position until T_e and T_i almost converge. The ionization state Z increases slightly along the axial position, ranging from approximately 3 to 4.

IV. DISCUSSION

The comprehensive analysis of moiré deflectometry, optical spectroscopy, and TS data allows for the evaluation of different plasma dimensionless numbers. The sonic Mach number as a function of axial position was determined for each opening angle ϕ , as shown in Fig. 9. It is observed that the plasma jet remains supersonic throughout the measured axial range, and the sonic Mach number increases with ϕ , following the relation $M_{s,\phi=20^\circ} < M_{s,\phi=30^\circ} < M_{s,\phi=40^\circ}$, in agreement with the corresponding velocity profiles.

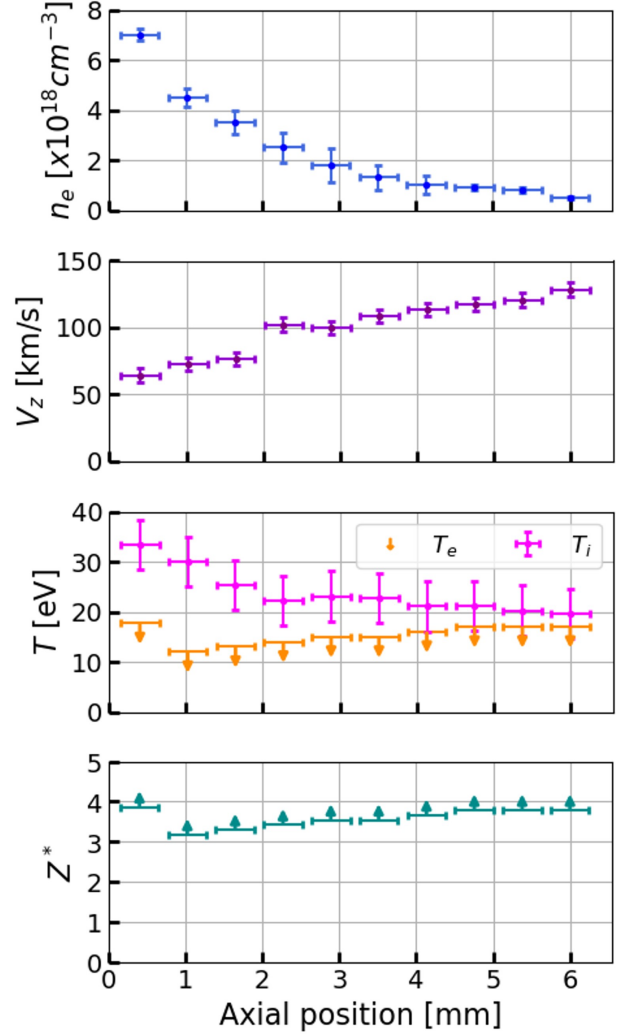


FIG. 8. Axial plasma parameter profiles of the jet emitted by a 40° opening angle conical wire array, 450ns after the beginning of current discharge.

To calculate global dimensionless numbers, we considered a set of characteristic plasma parameters of every plasma jet. These are evaluated considering $L_n = 2.86$ mm as the length scale. The characteristic plasma parameters considered and the dimensionless numbers obtained are presented in table I.

Consistent with Fig. 9, the plasma jet remains supersonic for all cone geometries. The large Reynolds number suggests that viscous dissipation occurs at scales much smaller than the system size, making viscous effects negligible for every ϕ . The magnetic Reynolds number indicates that the magnetic field is primarily advected, with magnetic diffusion becoming relevant only at smaller spatial scales. In addition, it shows a slight increase with larger cone opening angles. The small Knudsen number, defined as the ratio of the ion-ion mean free path to the characteristic length scale, confirms that ions within the plasma jet are highly collisional, regardless of the cone

Measured Parameter	Symbol	$\phi = 20^\circ$	Value $\phi = 30^\circ$	$\phi = 40^\circ$
Peak electron density [$\times 10^{18} \text{ cm}^{-3}$]	n_e	1.4 ± 0.6	1.8 ± 0.5	1.6 ± 0.5
Flow Velocity [km/s]	v	71 ± 5	89 ± 5	100 ± 5
Electron temperature [eV]	T_e	17 ± 3	15 ± 2	15 ± 2
Ion temperature [eV]	T_i	22 ± 5	23 ± 4	24 ± 4
Average ionisation	Z^*	3.7 ± 0.3	3.5 ± 0.2	3.5 ± 0.2
Dimensionless parameter				
Sonic Mach number	M_s	3.9 ± 0.4	5.0 ± 0.5	6 ± 0.5
Reynolds number [$\times 10^5$]	R_e	1.4 ± 0.6	1.5 ± 0.6	1.8 ± 0.4
Magnetic Reynolds number	R_{eM}	22 ± 4	30 ± 5	39 ± 6
Knudsen number [$\times 10^{-4}$]	K_n	3.1 ± 0.3	3.0 ± 0.4	3.4 ± 0.4
Peclet number [$\times 10^3$]	P_e	5.2 ± 0.3	6.7 ± 0.7	9.0 ± 0.6

TABLE I. Characteristic plasma parameters of the different ϕ jets at $z \approx 3\text{mm}$, $\sim 450\text{ ns}$ after current start. To evaluate the Reynolds, magnetic Reynolds and Peclet number, a scale length given by $L_n = 2.86\text{ mm}$ is considered

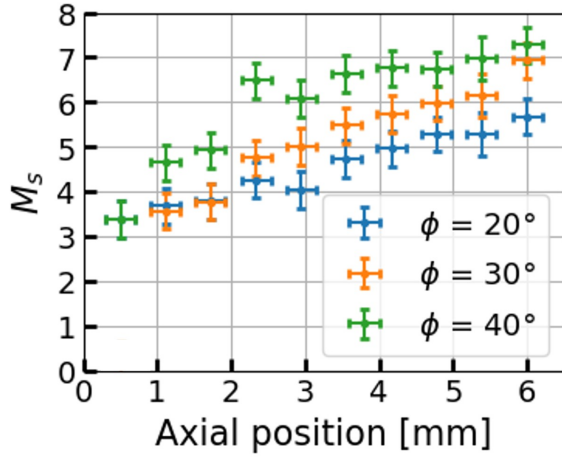


FIG. 9. Axial mach numer profile determined for the plasma jet, for three different opening angles.

geometry. Lastly, the Peclet number increases slightly with the opening angle but, in all cases, its high value suggests that thermal conductivity remains negligible at the characteristic spatial scale of the jet. Furthermore, relevant characteristic length scales can be determined. Table II presents relevant length scales calculated using the characteristic parameters of the $\phi = 30^\circ$ plasma jet.

To explain the observed temperature profiles, the competing mechanisms of heating, cooling, and transport are analyzed.

For an aluminium plasma in this density regime, radiative cooling becomes significant. The radiative cooling time is given by [26]

$$\tau_{cool} = 2.4 \times 10^{-12} \frac{(1 + Z)T_e}{Zn_z\Lambda(n_i, T_e)} \quad (1)$$

where $\Lambda(n_i, T_e)$ is the cooling function.

Combining numerical simulation presented in references [26–28] with the T_e and n_i measured in this

work, $\Lambda(n_i, T_e)$ is estimated and used to determine τ_{cool} . Fig.10a shows the cooling time for an aluminium plasma within the relevant electron temperature range and for different values of n_i . This shows that the plasma jet is efficiently cooled across the entire electron temperature range of interest. The jet exhibits stronger cooling for higher densities, which is consistent with colder electrons at the base of the jet, where the density is larger. The cooling efficiency decreases along the axis, according with a decrease in density for higher axial positions.

Moreover, Fig.10b compares the cooling time and ion-electron equilibration time $\tau_{eq}^{i/e}$ [29] with the plasma hydrodynamic time ($t_{hyd} = L_n/V_z$). Since $\tau_{eq}^{i/e} < t_{hyd}$, we would expect complete thermal equilibrium between ions and electrons. However, since $\tau_{cool} < \tau_{eq}^{i/e}$, electrons cool down before thermal equilibrium with the ions is reached. This leads to thermal decoupling between electrons and ions, which is consistent with the observed temperature profiles. Therefore, the ions are indirectly cooled via energy exchange with the electrons, which radiate energy away.

By comparing the temperature difference between the electrons and the ions at each axial position, with the difference between τ_{cool} and $\tau_{eq}^{i/e}$, the temperature profile can be fully described. The maximum difference between electron and ion temperatures is reached in the most dense zone of the jet, where $\tau_{cool} \ll \tau_{eq}^{i/e}$. While at higher axial positions of the jet, the thermal decoupling is minimum, where $\tau_{cool} \approx \tau_{eq}^{i/e}$. By considering this, the axial T_e profile observed in the TS data agrees with variations in cooling efficiency for different densities. A decrease in electron density along the axis allows the electrons to retain their temperature, resulting in an axial increase in electron temperature.

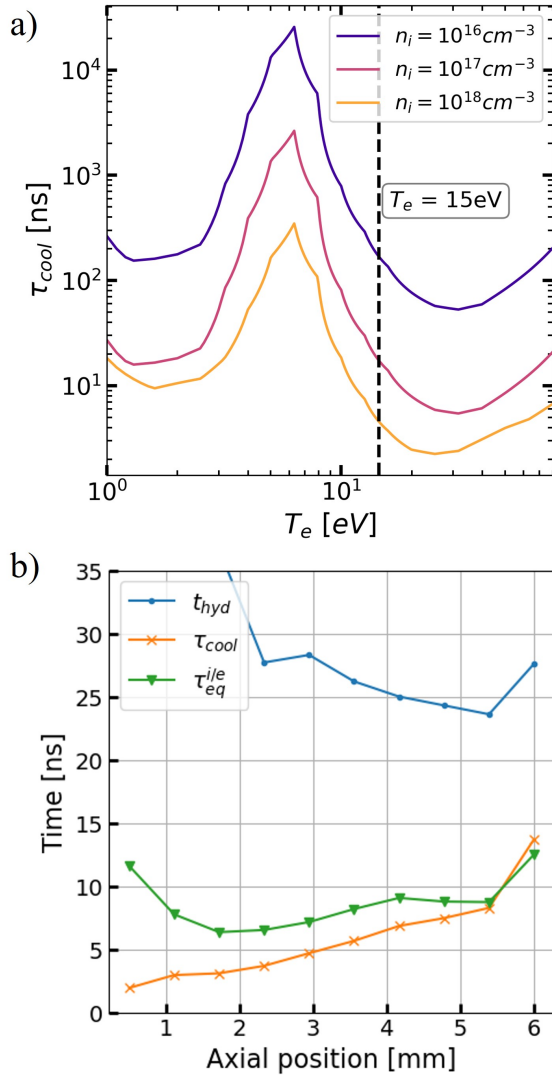


FIG. 10. a) Cooling time as a function of electron temperature for aluminium at different n_i . b) Time scales computed with the plasma parameters determined for each axial position.

Scale length	Symbol	Value (μm)
Internal ion-ion mean free path	$\lambda_{i,i}$	0.13
Resistive diffusion length	L_η	270
Electron thermal diffusion length	L_χ	90
Ion inertial length	d_i	0.3

TABLE II. Characteristic scale lengths calculated with the characteristic parameters of the $\phi = 30^\circ$ plasma jet presented in table I

V. CONCLUSIONS

In this work, we have performed a comprehensive experimental study of plasma jets emitted by aluminium conical wire arrays driven on the Llampudken pulsed power generator. By combining three complementary diagnostics, including moiré schlieren deflectometry,

optical emission spectroscopy, and Thomson scattering we achieved spatially resolved measurements of key plasma parameters, including electron density, flow velocity, and ion/electron temperatures.

Our results indicate that the inclusion of a physical aperture at the top of the conical array played a crucial role in isolating the jet from ablated plasma streams coming from the wires themselves. This modification altered the overall density profile observed in previous experiments using interferometry, revealing a jet with significant lower density than previously reported. We consider that these previous measurements have overestimated electron densities by adding both jet and ablation stream densities as a single flow.

For the jet itself, we have experimentally shown an exponential decay in axial electron density distribution with a characteristic axial scale length, L_n , which is consistent across different opening angles. Besides that, we found that as density and temperature profiles remain largely invariant with the array opening angle, the jet propagation velocity increases with ϕ , providing a straightforward way to control this parameter. The plasma jets are found to be supersonic, highly collisional, and in a regime where magnetic and thermal diffusion are negligible at the characteristic spatial scales. The axial temperature profile is shaped by the balance between ion-electron energy exchange and radiative cooling, with thermal decoupling appearing near the jet base due to higher density and enhanced radiative losses.

Since pulsed power plasma jets have often been used as laboratory astrophysics platforms, a more detailed description of internal parameters and their gradients along the plasma jet support their relevance in scalability to astrophysical systems such as young stellar object outflows and offer valuable benchmarks for simulations. As collisionality in plasmas is highly dependant on the velocity, these results also encourage the use of conical wire array jets as platform to study plasma collisionality taking advantage of known velocity values, their gradients, and the ϕ parameter as a way to control them.

Future work will also aim to expand the diagnostic capabilities by incorporating magnetic field measurements—specifically Zeeman spectroscopy—which will enable the determination of magnetic pressure, thermal and ram beta, Alfvénic Mach number, and additional length scales such as the ion and electron gyroradii. These measurements will further strengthen the connection between laboratory plasma jets and astrophysical outflows, allowing for more complete and accurate comparisons with theoretical models and simulations, as well as enabling the study of plasma-plasma interactions and the characterization of their collisionality regimes.

VI. ACKNOWLEDGEMENTS

This work has been partially funded by Fondecyt/Regular 1231286, 1220533, 3230401 and 1211131 projects. L. Izquierdo acknowledges doctoral funding from ANID-Subdirección de Capital Humano/Doctorado Nacional/2023-21230431.

-
- [1] D. S. De Young, “Astrophysical jets,” *Science*, vol. 252, no. 5004, pp. 389–396, 1991.
 - [2] C. J. Burrows, K. R. Stapelfeldt, A. M. Watson, J. E. Krist, G. E. Ballester, J. T. Clarke, D. Crisp, J. S. Gallagher III, R. E. Griffiths, J. J. Hester, *et al.*, “Hubble space telescope observations of the disk and jet of hh 30,” *The Astrophysical Journal*, vol. 473, no. 1, p. 437, 1996.
 - [3] B. Reipurth and J. Bally, “Herbig-haro flows: Probes of early stellar evolution,” *Annual Review of Astronomy and Astrophysics*, vol. 39, no. 1, pp. 403–455, 2001.
 - [4] K. W. Weiler and R. A. Sramek, “Supernovae and supernova remnants,” *IN: Annual review of astronomy and astrophysics. Volume 26 (A89-14601 03-90). Palo Alto, CA, Annual Reviews, Inc., 1988, p. 295-341.*, vol. 26, pp. 295–341, 1988.
 - [5] L. Izquierdo, F. Veloso, J. Valenzuela, M. Escalona, D. Oportus, and M. Favre, “Shock interactions between plasma jets from conical wire array z-pinches and laser-produced plasma plume,” *Results in Physics*, vol. 37, p. 105476, 2022.
 - [6] S. Lebedev, J. Chittenden, F. Beg, S. Bland, A. Ciardi, D. Ampleford, S. Hughes, M. Haines, A. Frank, E. Blackman, *et al.*, “Laboratory astrophysics and collimated stellar outflows: The production of radiatively cooled hypersonic plasma jets,” *The Astrophysical Journal*, vol. 564, no. 1, p. 113, 2002.
 - [7] S. V. Lebedev, A. Ciardi, D. J. Ampleford, S. Bland, S. C. Bott, J. P. Chittenden, G. N. Hall, J. Rapley, C. Jennings, M. Sherlock, *et al.*, “Production of radiatively cooled hypersonic plasma jets and links to astrophysical jets,” *Plasma Physics and Controlled Fusion*, vol. 47, no. 12B, p. B465, 2005.
 - [8] A. Ciardi, S. V. Lebedev, A. Frank, F. Suzuki-Vidal, G. N. Hall, S. N. Bland, A. Harvey-Thompson, E. G. Blackman, and M. Camenzind, “Episodic magnetic bubbles and jets: astrophysical implications from laboratory experiments,” *The Astrophysical Journal*, vol. 691, no. 2, p. L147, 2009.
 - [9] S. Bott-Suzuki, L. Caballero Bendixsen, S. Cordaro, I. Blesener, C. Hoyt, A. Cahill, B. Kusse, D. Hammer, P. Gourdain, C. Seyler, *et al.*, “Investigation of radiative bow-shocks in magnetically accelerated plasma flows,” *Physics of Plasmas*, vol. 22, no. 5, 2015.
 - [10] E. Lavine, D. Lund, E. Freeman, W. Potter, C. Seyler, and B. Kusse, “An experimental platform for investigating astrophysically relevant magnetized plasma jets on the cobra facility,” *Physics of Plasmas*, vol. 32, no. 1, 2025.
 - [11] F. Veloso, G. Muñoz-Cordovez, L. Donoso-Tapia, V. Valenzuela-Villasaca, M. Favre, and E. Wyndham, “Plasma outflows from wire-based z-pinch experiments driven at currents of hundreds of kiloamperes,” in *Journal of Physics: Conference Series*, vol. 720, p. 012039, IOP Publishing, 2016.
 - [12] S. Lebedev, D. Ampleford, S. Bland, J. Chittenden, A. Ciardi, N. Naz, M. Haines, A. Frank, E. Blackman, and T. Gardiner, “Experiments with radiatively cooled supersonic plasma jets generated in conical wire array z-pinches,” in *2002 14th International Conference on High-Power Particle Beams (BEAMS)*, vol. 2, pp. 317–320, IEEE, 2002.
 - [13] A. Ciardi, S. Lebedev, J. Chittenden, and S. Bland, “Modeling of supersonic jet formation in conical wire array z-pinches,” *Laser and Particle Beams*, vol. 20, no. 2, pp. 255–261, 2002.
 - [14] A. Ciardi, S. V. Lebedev, A. Frank, F. Suzuki-Vidal, G. N. Hall, S. N. Bland, A. Harvey-Thompson, E. G. Blackman, and M. Camenzind, “Episodic magnetic bubbles and jets: astrophysical implications from laboratory experiments,” *The Astrophysical Journal*, vol. 691, no. 2, p. L147, 2009.
 - [15] F. Suzuki-Vidal, S. Lebedev, M. Krishnan, J. Skidmore, G. Swadling, M. Bocchi, A. Harvey-Thompson, S. Patankar, G. Burdiak, P. de Grouchy, *et al.*, “Interaction of radiatively cooled plasma jets with neutral gases for laboratory astrophysics studies,” *High Energy Density Physics*, vol. 9, no. 1, pp. 141–147, 2013.
 - [16] H. Chuaqui, E. Wyndham, C. Friedli, and M. Favre, “Llampüdkeñ: A high-current, low-impedance pulser employing an auxiliary exponential transmission line,” *Laser and Particle Beams*, vol. 15, no. 2, pp. 241–248, 1997.
 - [17] I. H. Hutchinson, “Principles of plasma diagnostics,” *Plasma Physics and Controlled Fusion*, vol. 44, no. 12, pp. 2603–2603, 2002.
 - [18] J. Valenzuela, E. Wyndham, H. Chuaqui, D. Cortes, M. Favre, and H. Bhuyan, “Implementation of moiré-schlieren deflectometry on a small scale fast capillary plasma discharge,” *Journal of Applied Physics*, vol. 111, no. 10, 2012.
 - [19] C. J. Dasch, “One-dimensional tomography: a comparison of abel, onion-peeling, and filtered backprojection methods,” *Applied optics*, vol. 31, no. 8, pp. 1146–1152, 1992.
 - [20] M. P. Valdivia, G. Pérez-Callejo, L. Izquierdo, F. Veloso, A. Truong, H. Hu, N. Dilworth, S. C. Bott-Suzuki, and V. Bouffetier, “z-pinch interferometry analysis with the fourier-based tnt code,” *IEEE Transactions on Plasma Science*, 2024.
 - [21] D. W. Hahn and N. Omenetto, “Laser-induced breakdown spectroscopy (libs), part i: review of basic diagnostics and plasma-particle interactions: still-challenging issues within the analytical plasma community,” *Applied spectroscopy*, vol. 64, no. 12, pp. 335A–366A, 2010.

- [22] R. H. Huddleston, S. L. Leonard, and H. P. Furth, "Plasma diagnostic techniques," 1966.
- [23] D. Dojić, M. Skočić, S. Bukvić, and S. Djeniže, "Stark broadening measurements of al ii, al iii and he i 388.86 nm spectral lines at high electron densities," *Spectrochimica Acta Part B: Atomic Spectroscopy*, vol. 166, p. 105816, 2020.
- [24] M. Escalona, J. Valenzuela, G. Avaria, F. Veloso, and E. Wyndham, "Bayesian inference of plasma parameters from collective thomson scattering technique on a gas-puff near stagnation," *Scientific Reports*, vol. 13, no. 1, p. 13002, 2023.
- [25] D. H. Froula, S. H. Glenzer, N. C. Luhmann Jr, J. Sheffield, and T. J. Donné, "Plasma scattering of electromagnetic radiation: theory and measurement techniques," 2012.
- [26] F. Suzuki-Vidal, S. Lebedev, A. Ciardi, L. Pickworth, R. Rodriguez, J. Gil, G. Espinosa, P. Hartigan, G. Swadling, J. Skidmore, *et al.*, "Bow shock fragmentation driven by a thermal instability in laboratory astrophysics experiments," *The Astrophysical Journal*, vol. 815, no. 2, p. 96, 2015.
- [27] D. R. Russell, *Bow shock interaction experiments in a magnetised collisional plasma*. PhD thesis, Imperial College London, 2021.
- [28] V. Valenzuela-Villasaca, L. G. Suttle, F. Suzuki-Vidal, J. W. Halliday, D. R. Russell, S. Merlini, E. R. Tubman, J. D. Hare, J. P. Chittenden, M. E. Koepke, *et al.*, "On the structure of plasma jets in the rotating plasma experiment," *IEEE Transactions on Plasma Science*, 2024.
- [29] A. Richardson and N. P. Formulary, "Us naval research laboratory," 2019.